# IN-SITU MEASUREMENT AND VISUALIZATION OF ELECTROMAGNETIC FIELDS

Satoshi Yagitani, Mitsunori Ozaki
*Institute of Science and Engineering, Kanazawa University, Kakuma-machi, Kanazawa, Japan*
yagitani@is.t.kanazawa-u.ac.jp, ozaki@is.t.kanazawa-u.ac.jp

Yoshiyuki Yoshimura, Hirokazu Sugiura
*Industrial Research Institute of Ishikawa, 2-1 Kuratsuki, Kanazawa, Japan*
yyoshi@irii.jp, h-sugiura@irii.jp

Keywords: Electromagnetic fields, Radio-frequency fields, Measurement, Visualization, EMC, Absorber.

Abstract: In-situ monitoring of electromagnetic field distributions is useful for localizing and identifying EM noise sources, as well as for evaluating actual antenna characteristics. A couple of new techniques developed for in-situ measurement and visualization of electromagnetic fields are reported. At first, visualization of EM field distributions measured by a freehand scanning sensor on a live video image is described. Secondly, imaging of 2-d RF field distributions incident on a metamaterial absorber is explained. Then, in-situ visualization techniques for EM vectors and RF polarizations are discussed. Such techniques are expected to be quite useful for measuring EM field distributions in various scenarios in the fields of EMC, antennas and propagation.

## 1 INTRODUCTION

In-situ measurement of the actual spatial distributions of electromagnetic (EM) field is useful for localizing and identifying EM noise sources in electric or electronic equipment under actual operating conditions, as well as for evaluating the performance of antennas in wireless communication devices used in real environments. Conventionally, the spatial distributions of the EM field have been measured by scanning the plane/volume of interest with a sensor or sensor array. So far there have been proposed and developed a wide variety of mapping and cartography systems of EM distributions from the viewpoint of EMC/EMI. For radio-frequency (RF) fields from tens of MHz up to tens of GHz, various kinds of sensor-scanning systems have been developed to measure RF emissions from electronic devices and systems, individual PCBs, and even onboard VLSI chips. In these systems, for example, an electric field probe (Dutta et al., 1999), a magnetic loop probe (Haelvoet et al, 1996), a magnetic sensor array (Yamaguchi et al., 1999), and an electromagnetic field probe (Kazama and Arai, 2002) have been used with mechanically-scanning systems (Baudry et al., 2007), which have measured and visualized RF near-field distributions. A 2-d dense array of thousands of loop sensors for near-field distribution imaging (without the need for scanning) has also been available (Fan, 2009). The near-field distributions have been used to identify radiated emission sources (Laurin et al., 2001) and to predict far-field noise radiation (Shi et al., 2004). Another study has measured Fresnel near-field distributions to holographically localize RF leakage points for example from a shielded door (Kitayoshi and Sawaya, 1999) and from the surface of spacecraft (Chen et al., 2012).

It is noted that for dc to low-frequency magnetic field application, there have been independently developed the imaging systems such as “magnetovision” with scanning 1d and 2d magnetoresistive (MR) sensor arrays, to obtain principally dc magnetic field images, for example for investigation of magnetized materials (Tumanski and Liszka, 2002; Tumanski and Baranowski, 2006).

Another unique RF field imaging technique has been proposed which employs an infrared (IR)



Yagitani S., Ozaki M., Yoshimura Y. and Sugiura H.
IN-SITU MEASUREMENT AND VISUALIZATION OF ELECTROMAGNETIC FIELDS.
DOI: 10.5220/0004784700210029
In *Proceedings of the Second International Conference on Telecommunications and Remote Sensing (ICTRS 2013)*, pages 21-29
ISBN: 978-989-8565-57-0

thermogram (Norgard and Musselman, 2004). An RF field impinging on a lossy screen is absorbed and creates a temperature rise there corresponding to a map of absorbed power distribution, which is taken by an IR camera. A "live electro-optic (EO) imaging" system has employed an ultra-parallel photonic heterodyne technique to take a video image of electric near-field distribution applied on an EO crystal plate at microwave frequencies (Sasagawa et al., 2007). The electric fields more than tens of GHz were down-converted and lively displayed at 30 frames/second as a 2d image with 100x100 pixels.

Generally these techniques give accurate cartographic mapping and images of EM fields, but require specific sensor scanning devices or imaging systems. In constrast, the authors' group have been developing compact in-situ measurement and visualization techniques for EM fields, which could be used to capture an intuitive view of EM distributions existing in actual environments. In this paper a couple of developed techniques to measure and visualize EM field distributions are reported.


Figure 1: EM field distribution imager.

## 2 EM FIELD MEASUREMENT AND VISUALIZATION ON A VIDEO IMAGE

### 2.1 EM Field Distribution Imager

The "EM field distribution imager" illustrated in Figure 1 measures and visualizes in-situ EM field distributions on a live video image of the real world. The image of an EM sensor is taken by a single video camera. Image processing is applied on a PC and the location of the sensor is identified on each frame of the video image, where the sensor location is painted with the color representing the EM field intensity actually measured by the sensor itself. By freely scanning the sensor by hand, the image of the in-situ field distribution is gradually showing up along the sensor trajectory as a color map on the video image. Figure 2 shows an example of the RF field (1.9 GHz) visualization around a mobile phone. A sleeve dipole antenna was put inside a yellow acrylic spherical cover of 10 cm diameter. A video camera was placed 1 m away from the cell phone put on a tripod in an office room. Here the 3d location of the sensor was identified by extracting the yellow circle on the image, the center and size of which gave information on the sensor's lateral and depth location relative to the camera. Along the freely scanned trajectory an intensity map of the RF filed was created, which exhibited a standing-wave pattern possibly caused by reflection at the wall or floor. With this system one can scan the space of interest while watching the video image, to obtain an intuitive view of EM field distribution, in every situation wherever the video camera and the sensor can be carried in.

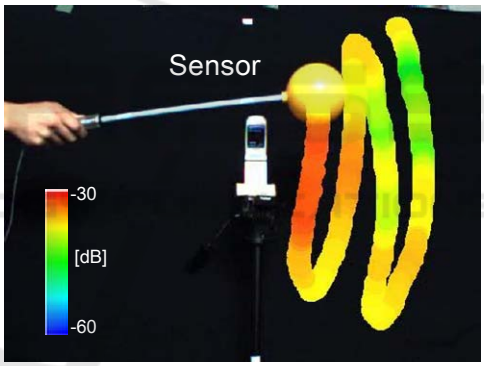


Figure 2: RF field imaging around a mobile phone.

This kind of freehand-scanning method has been developed also by other researchers, based on magnetic tracking, optical tracking and IR tracking, for the investigation of the low-frequency magnetic noise emitted from electrical appliance (Sato et al., 2010; Sato et al., 2012).

### 2.2 Magnetic Field Vector Imaging and Source Current Estimation

Even with a single video camera, this system can determine the sensor's 3d orientation in addition to its 3d location, by putting a specific marking on the spherical sensor cover. One way is to paint three marks with different colors indicating the three axial directions of the internal sensor, which are

recognized on the video image to calculate the sensor orientation. This makes it possible to measure EM vector directions when we use an EM vector sensor. Figure 3 (a) shows an example of the magnetic field vectors measured and visualized around a 45x45-cm square loop antenna (10 kHz, 63 mA-Turns), where the 2d projection of the measured 3d vectors are plotted with length and color indicating the field intensity. Though not shown here a tri-axial magnetic search-coil sensor was used; three 10-cm-long uni-axial sensors were placed orthogonally with each other, covered by a 15-cm acrylic sphere. A perpendicular plane 1 m away from the camera (and 9 cm in front of the loop plane) was manually scanned by the sensor. Measurement was done at 7x7=49 points on a 60x60 cm area. Compared with theoretically calculated values, the measured errors in intensity and vector direction of the magnetic field were less than 10% and 10 degrees, respectively. These errors were caused by the errors in location (3 cm) and in orientation (a few degrees) of the sensor which was identified on a 640x480-pixel video image.

From the measured magnetic field vectors the source current distributions were estimated by the GVSPM method on the plane including the loop source (Yagitani et al., 2007). Figures 3 (b) and (c) plot the estimated source current vectors and amplitudes on the loop plane. The estimated current vectors are visualized on the real image of the loop source, where the estimated current is practically reconstructed along the actual square route of the loop current. Thus, the free-scanning system is expected to contribute not only to imaging of EM field distributions but also estimating their sources.

## 2.3 EM Imaging by Smartphone and Tablet PC

The measurement and visualization technique has also been implemented onto a smartphone and tablet PC. Figure 4 shows an example of a low frequency (60 Hz) magnetic field distribution around an electric cooker, which was measured by a magnetic sensor with an augmented reality (AR) tag attached, and visualized on a smartphone screen. With these up-to-date devices, built-in cameras are used to take a video image, while they can easily communicate with the sensors through wireless links. Furthermore an open-source AR software makes it easy to implement the sensor identification capability on the video image in a smartphone/tablet app.

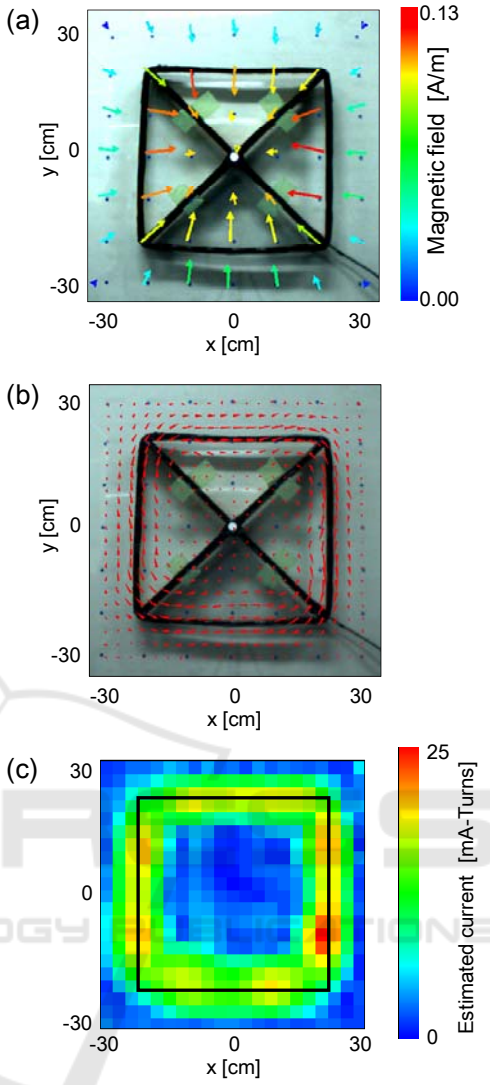


Figure 3: Low-frequency magnetic field vectors and estimated current distribution: (a) measured magnetic field vector distribution, (b) estimated current vectors, (c) estimated current amplitude distribution.


Figure 4: Low-frequency magnetic fields from an electric cooker, measured by a magnetic sensor with an AR tag attached, and visualized on a smartphone screen.

# 3 RF FIELD DISTRIBUTION IMAGER USING METAMATERIAL ABSORBER

## 3.1 Metamaterial Absorber

It has been proposed that a metamaterial absorber could be used for monitoring 2d power distributions of a radio-frequency (RF) wave incident on the absorber surface (Yagitani et al., 2011a). The metamaterial absorber was designed by employing a mushroom-type electromagnetic band-gap (EBG) structure used as a high-impedance surface (alternatively called an artificial magnetic conductor). As shown in Figure 5 (a), a 2d matrix of dense square metal patches formed on a dielectric substrate were connected to the ground plane through vias. Lumped resistors interconnecting the square patches were placed on the surface to absorb the incident wave (Gao et al., 2005). A simple equivalent circuit based on the transmission line model for the absorber is shown in Figure 5 (b); the capacitance $C$ is formed between the adjacent patches whereas the inductance $L$ comes from the wave propagation (transmission line) inside the substrate (Luukkonen et al., 2009). At the resonance frequency the LC impedance becomes infinite so that the surface resistance $R$ absorbs the incident wave if $R$ is matched with the free space wave impedance, 377 Ω, for normal incidence. Figure 5 (c) shows the reflection and absorption characteristics; the maximum absorption (minimum reflection) occurs at the resonance frequency. Since $L$ and $C$ are determined by the metamaterial structure, varactor diodes were inserted parallel to the resistors to make the resonance (absorption) frequency tunable (Mias and Yap, 2007).

## 3.2 RF Power Distribution Measurement

The configuration of this kind of metamaterial absorber makes it possible to directly measure the amounts of power absorbed (or consumed) by the individual lumped resistors. As in Figure 6, an RF power detector can be attached to each resistor and measure the absorbed power. A 2d array of power detectors attached to the lumped resistors are used to capture the 2d image of the RF power incident and absorbed on the surface. The amount of power absorbed by each resistor is dependent on the incident polarization; the incoming RF waves with the electric field polarized in the $x$- and $y$-directions are absorbed by the resistors connecting the adjacent patches in the $x$- and $y$-directions, respectively. In either case, the power absorbed by each resistor is considered to be the Poynting flux of the incident wave multiplied by the area of one unit cell. Thus, the information on the incident polarization is obtained by the power detectors individually attached to the $x$- and $y$-resistors.

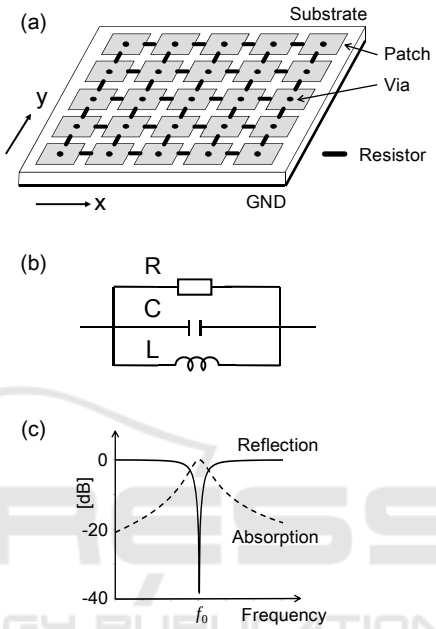


Figure 5: A metamaterial absorber: (a) basic structure, (b) equivalent circuit, and (c) reflection and absorption characteristics.

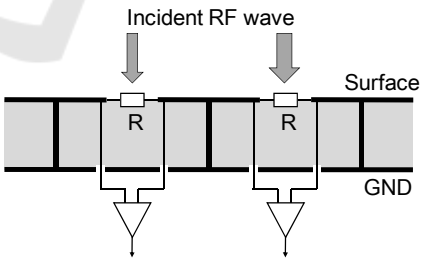


Figure 6: Measurement of absorbed RF power

A metamaterial absorber was designed and fabricated which was made tunable between 700 MHz and 2.7 GHz (Yagitani et al., 2011a). A 33x33 array of square unit cell were formed on an FR-4 substrate of 347 mm square and 1.6 mm thick. The size of each patch was 10 mm and the gap between the adjacent patches was 0.5 mm. Lumped resistors (620 Ω) and RF varactor diodes (Infineon BB833)

were inserted in parallel between the patches. The equivalent circuit model of the absorber is given in Figure 7, where $C_D$, $L_D$ and $R_D$ are the stray capacitance, stray inductance and resistance of a varactor diode, respectively, and $R_{loss}$ represents the dielectric loss of the substrate. Detailed analysis of such a circuit was made to reveal that even a small varactor resistance (a few Ohms) is translated to a larger surface resistance which severely degrades the absorption performance especially at lower frequencies (Yagitani et al., 2011b). The performance of the absorber is shown in Figure 8 (with data taken from Yagitani et al., 2011a), where a black solid line, a gray line and a broken line represent the measured profile, the profiles obtained by equivalent-circuit analysis and EM simulation (CST MW-STUDIO), respectively. These profiles practically agree with each other. The symbols A, B, C and D correspond to the varactor capacitances of 3.35 pF, 1.72 pF, 1.09 pF and 0.72 pF, respectively. Here the lumped resistors had been chosen as 620 Ω so that the maximum absorption was obtained at 2.62 GHz.

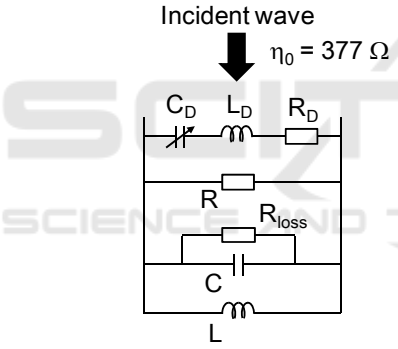


Figure 7: Equivalent circuit model of the fabricated metamaterial absorber.

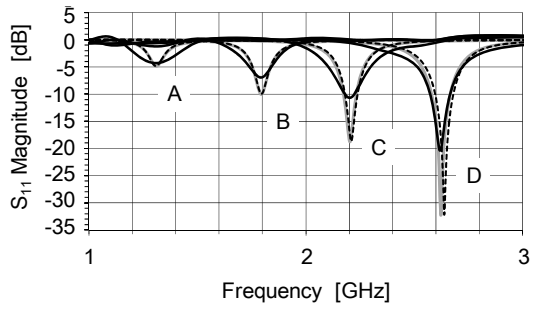


Figure 8: Absorption performance of the fabricated metamaterial absorber (data from Yagitani et al., 2011a).

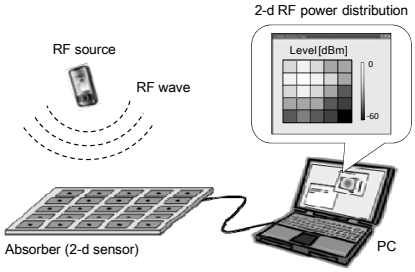


Figure 9: RF power distribution imager.

Using the fabricated absorber an RF power imager was developed, as schematically illustrated in Figure 9. The RF power distribution incident on the surface was detected by an array of power detectors attached on the backside of the absorber. An array of 64 power detectors were arranged in a 8x8 matrix to measure the *x*-polarization, whereas another array of 64 detectors were placed for the *y*-polarization. A logarithmic power detector (Analog Devides, ADL5513) was used, which measures the power in the range from -70 dBm to +10 dBm between 1 MHz and 4 GHz. The detected RF power distribution was A/D converted, transferred to a PC and displayed as a 2d color map at 30 images/second.

With this system, RF power distributions radiated from a standard dipole antenna were measured in the experimental setup shown in Figure 10 (a). A horizontally polarized radio wave (0 dBm) at 2.2 GHz was transmitted from the antenna placed at a distance *d* from the absorber. Figure 10 (b) plots the measured power distribution of horizontal polarization at $d$ = 10 cm. An elliptic power distribution corresponding to the directivity of the horizontal dipole was captured. The power distributions along the *x*- and *y*-axes are compared with the theoretical values in Figure 10 (c), which were calculated according to the previous work (Yagitani et al., 2011a). Here each power detector had been calibrated by an almost far-field and plane-wave pattern, created by the transmitting antenna placed at $d$ = 80 cm. For distances of $d$ = 30 cm and 50 cm, the measured profiles practically agree with the theoretical curves. At a distance of 10 cm, however, the measured profiles became weaker than the theoretical ones. This would be caused by that at this short distance the radiated field did not completely become a far-field so that impedance mismatch caused the reflection from the absorber surface. More rigorous treatment for near-field spherical wave incidence is needed to quantitatively discuss the accuracy of power distributions at such a short distance.

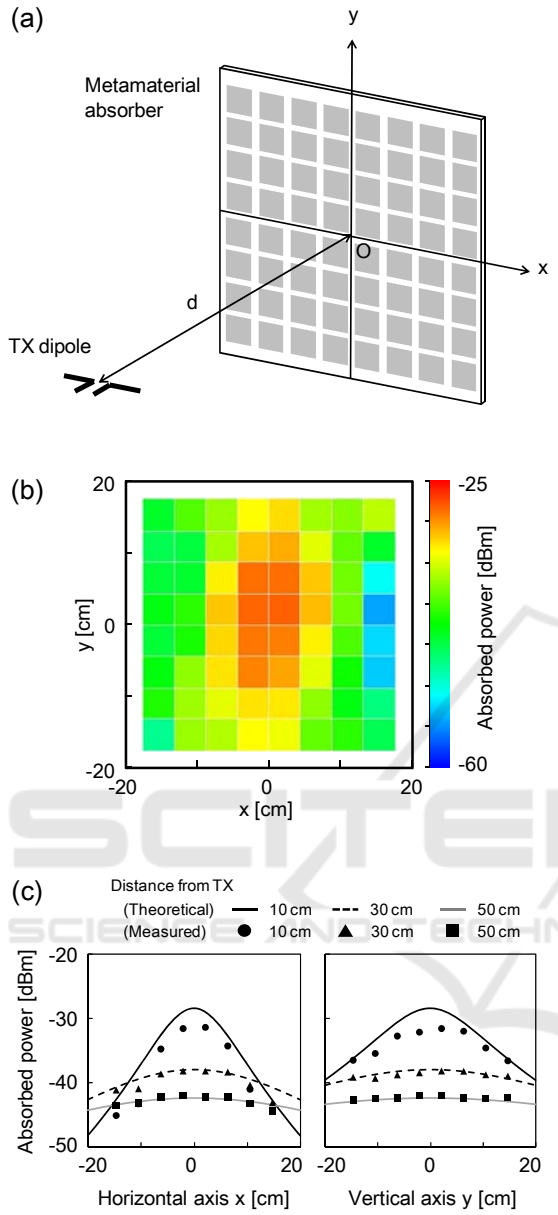


Figure 10: Measurement of RF power distribution: (a) experimental setup, (b) power distribution at 10 cm from the transmitter, and (c) horizontal and vertical profiles of power distribution.

### 3.3 RF Amplitude and Phase Distribution Measurement

On the basis of the developed technique, RF amplitude and phase distributions can also be obtained. By measuring the amplitude and phase of the voltages induced on each individual resistor, we are able to calculate those of the electric field incident upon it. This has been quantitatively confirmed by simulation (Yagitani et al., 2013). However, it was revealed that edge reflection from a finite-sized absorber created a specific interference pattern on the amplitude and phase profiles on the absorber surface, thereby degrading the accuracy of the measurement. Though the interference pattern depended on the absorber size and frequency, generally the central area of the absorber had the highest measurement accuracy (less than 10% errors). Reduction in the edge reflection should be desired for practical use of this technique.

One application of amplitude and phase measurement is polarization identification. As explained in Section 3.2, the metamaterial absorber measures independently two orthogonal polarizations in the *x*- and *y*-directions. From the phase information in addition to the amplitude, linear, circular and elliptical polarizations are identified, including their major and minor axial directions as well as their sense of polarization, i.e., right- or left-handed (see also Section 4.2).

Another application is the direction finding and localization of RF sources. Ideally, when an incident RF wave is completely absorbed, each individual resistor (being as an amplitude and phase sensor) does not act as a scatterer so that no mutual coupling between the resistors is expected. Therefore the matrix of resistors on the absorber would work as an ideal antenna array. The present technique could be applied to obtaining the directions-of-arrival (DOAs) of the incoming RF signals from far sources, invoking various DOA estimation techniques such as MUSIC, ESPRIT, and others. The estimated source directions could even be visualized on a real image (Kwakkernaat et al., 2008). Source localization will be realized also for near-field sources. The near-field localization techniques such as radio holography (Kitayoshi and Sawaya, 1999), MUSIC (Kato et al., 2005) and SPM (Yoshimoto et al., 2005) could be used to obtain source locations and shapes, along with source visualization (Taira et al., 2004).

## 4 IN-SITU VISUALIZATION OF ELECTROMAGNETIC FIELDS

In general, an EM sensor measures an EM field and converts it to electric signals, which are then transferred to receivers, and processed and displayed on a PC when necessary. The authors have been working to develop the EM sensor having the capability of visualizing the measured field

immediately adjacent to the sensor itself, thereby one could intuitively figure out the in-situ field properties such as the intensity, vector direction and polarization. In this chapter new techniques under development based on this concept are described.

## 4.1 Electromagnetic Vector Compass

One example of such a system is an "Electromagnetic Vector Compass." The 3d vector direction of the in-situ EM field measured by an EM vector sensor is displayed on the surface of the sensor housing itself, as illustrated in Figure 11. Figure 12 shows a prototype of the vector compass for low-frequency AC magnetic field. A tri-axial search coil sensor is used to measure magnetic field vectors, which are processed by built-in receivers and displayed on an OLED screen attached on each of the six surfaces of the cubic housing. The screen on each surface plots an arrow representing the projection of the measured 3d vectors onto that surface. Just like an ordinary magnetic compass (for dc magnetic field), it displays in-situ EM vectors in real-time. With this kind of compact sensor one is able to observe the magnetic vectors in his/her hand, just at the point of measurement.

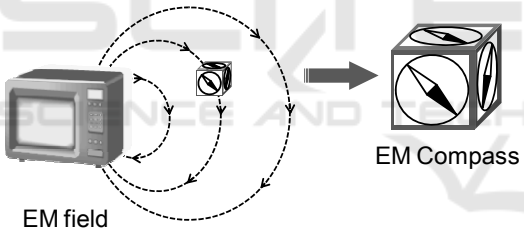


Figure 11: Electromagnetic vector compass.

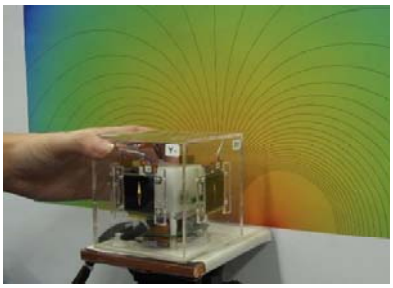

Figure 12: AC magnetic vector compass.

## 4.2 In-situ RF imaging Screen

In-situ visualization of RF fields is more difficult, since the sensor itself, cables, receivers and displays may reflect, scatter and disturb the field of interest. As explained in Chapter 3, we have developed a metamaterial absorber capable of measuring incident RF power, amplitude and phase distributions. If the absorber is made of transparent materials and a display screen is placed just behind it, we would be able to construct an "in-situ RF imaging screen" as illustrated in Figure 13. The 2d distribution of RF field absorbed on the surface is measured by embedded power (or amplitude and phase) detectors, which is transferred to the display and immediately visualized there. Thus the image of RF field is visualized in-situ, just as if a wall is illuminated by a flashlight.

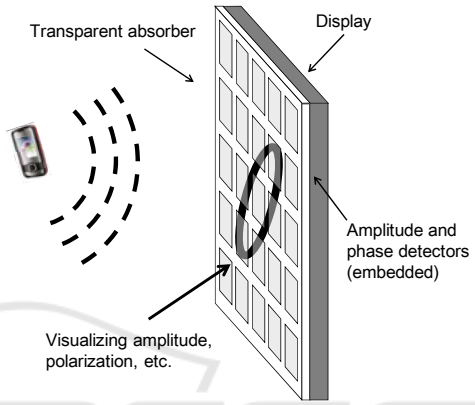


Figure 13: In-situ RF imaging screen.

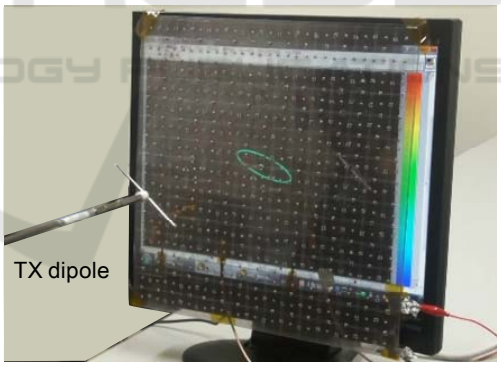


Figure 14: In-situ visualization of RF polarization.

A transparent absorber was fabricated, employing a transparent acrylic substrate and a transparent sheet of fine metal mesh. Transparent resistive films usually used to realize transparent absorbers (e.g., Haruta et al., 2000) were not adopted here because they have resistivity to absorb the RF field by themselves, whereas in the present absorber the RF power should be dissipated mainly in the lumped resistors. The size of the absorber was 30 cm square with 2-mm thickness. On the backside of the absorber amplitude and phase detectors were attached to measure two orthogonal polarizations.

Figure 14 shows a preliminary demonstration of in-situ visualization of polarization. A 1.7-GHz wave was transmitted from a dipole antenna and measured by the transparent absorber. The measured polarization at the center of the absorber was plotted on a PC display placed just behind the absorber. In this case the transmitted wave became an elliptically polarized, possibly due to the reflection from the table or cables.

# 5 CONCLUSIONS

Various in-situ measurement and visualization techniques and systems for EM fields were reported which have been developed by the authors' group. Using the developed systems, the EM fields can be captured and visualized in situ and in real-time. Such systems are expected to be quite useful for measuring EM field distributions in various scenarios in the fields of EMC, antennas and propagation. The systems could be applicable to quick noise measurement at the development stage of electric or electronic equipment, as well as to the in-situ measurement of EM field distributions in the actual environments such as offices, factories, cars, trains and airplanes. Last but not least, such visualization techniques could contribute to education in electromagnetics and radio engineering, where students will be able to virtually observe the actual EM fields in various situations.

# ACKNOWLEDGEMENTS

The authors would like to thank (ex-) students of Kanazawa University: Messrs. Y. Yamanaka, T. Shimizu, S. Morita, K. Katsuda, E. Tanaka, R. Tanaka, M. Nojima, S. Shiraki, T. Nakagawa, T. Sunahara, D. Hiraki, K. Iwasaki, N. Fukuoka and H. Maeda for their help with design, fabrication and measurement of the EM and RF measurement and imaging systems.

# REFERENCES

Baudry, D., Arcambal, C., Louis, A., Mazari, B., Eudeline, P., 2007. Applications of the near-field techniques in EMC investigations, *IEEE Trans. Electromagnetic Compatibility*, vol.49, no.3, pp.485-493.

Chen, H., Zhang, H., Ni, Z., Li, R., 2012. Research on imaging detection of RF leakage on the surface of spacecraft, *Proc. 2012 Int. Symp. EMC (EMC EUROPE)*, pp.1-4.

Dutta, S. K., Vlahacos, C. P., Steinhauer, D. E., Thanawalla, A. S., Feenstra, B. J., Wellstood, F. C., Anlage, S. M., Newman, H. S., 1999. Imaging microwave electric fields using a near-field scanning microwave microscope, *Applied Physics Letters*, vol.74, no.1, pp.156-158.

Fan, H., 2009. Far field radiated emission prediction from magnetic near field magnitude-only measurements of PCBs by Genetic Algorithm, *Proc. IEEE Int. Symp. EMC*, pp.321-324.

Gao, Q., Yin, Y., Yan, D.-B., Yuan, N.-C., 2005. A novel radar-absorbing-material based on EBG structure, *Microwave and Optical Technology Letters*, vol.47, no.3, pp.228-230.

Haelvoet, K., Criel, S., Dobbelaere, F., Martens, L., De Langhe, P., De Smedt, R., 1996. Near-field scanner for the accurate characterization of electromagnetic fields in the close vicinity of electronic devices and systems, *Proc. IEEE Instrumentation and Measurement Technology Conf.*, pp.1119-1123.

Haruta, M., Wada, K., Hashimoto, O., 2000. Wideband wave absorber at X frequency band using transparent resistive film, *Microwave and Optical Technology Letters*, vol.24, no.4, pp.223-226.

Kato, T., Taira, K., Sawaya, K., Sato, R., 2005. Estimation of short range multiple coherent source location by using MUSIC algorithm, *IEICE Trans. Commun.*, vol.E88-B, no.8, pp.3317-3320.

Kazama, S., Arai, K. I., 2002. Adjacent electric field and magnetic field distribution measurement system, *Proc. IEEE Int. Symp. EMC*, vol.1, pp.395–400.

Kitayoshi, H., Sawaya, K. 1999. Electromagnetic-wave visualization for EMI using a new holographic method, *Electronics and Communications in Japan, Part 1*, vol.82, no.8, pp.52-60.

Kwakkernaat, M. R. J. A. E., de Jong, Y. L. C., BuItitude, R. J. C., Herben, M. H. A. J., 2008. High-resolution angle-of-arrival measurements on physically-nonstationary mobile radio channels, *IEEE Trans. Antennas and Propagation*, vol.AP-56, no.8, pp. 2720-2729.

Laurin, J. J., Ouardhiri, Z., Colinas, J., 2001. Near-field imaging of radiated emission sources on printed-circuit boards, *Proc. IEEE Int. Symp. EMC*, vol.1, pp.368-373.

Luukkonen, O., Costa, F., Simovski, C. R., Monorchio, A., Tretyakov, S. A., 2009. A thin electromagnetic absorber for wide incidence angles and both polarizations, *IEEE Trans. Antennas and Propagation*, vol.57, no.10, pp.3119-3125.

Mias, C., Yap, J. H., 2007. A varactor-tunable high impedance surface with a resistive-lumped-element biasing grid, *IEEE Trans. Antennas and Propagation*, vol.55, no.7, pp.1955-1962.

Norgard, J., Musselman, R., 2004. CEM code validation using infrared thermograms, *Proc. 2004 Int. Symp. EMC*, pp.637-640.

Sasagawa, K., Kanno, A., Kawanishi, T., Tsuchiya, M., 2007. Live electrooptic imaging system based on ultraparallel photonic heterodyne for microwave near-fields, *IEEE Trans. Microwave Theory Tech.*, vol.55, no.12, pp.2782-2791.

Sato, K., Miyata, N., Kamimura, Y., Yamada, Y., 2010. A freehand scanning method for measuring EMF distributions using magnetic tracker, *IEICE Trans. Commun.*, vol.E93-B, no.7, pp.1865-1868.

Sato, K., Kawata, H., Kamimura, Y., 2012. A freehand scanning method for measuring EMF distributions, *IEICE Trans. Commun.*, vol.J95-B, No.2, pp.293-301. (in Japanese)

Shi, J., Cracraft, M. A., Zhang, J., DuBroff, R. E., Slattery, K., 2004. Using near-field scanning to predict radiated fields, *Proc. IEEE Int. Symp. EMC*, pp.14-18.

Taira, K., Kato, T., Sawaya, K., Sato, R., 2004. Estimation of source location of leakage field from transformer-type microwave oven, *Proc. 2004 Int. Symp. EMC*, vol.2, pp.489-493.

Tumanski, S., Liszka, A., 2002. The methods and devices for scanning of magnetic fields, *J. Magnetism and Magnetic Materials*, vol.242–245, pp.1253–1256.

Tumanski, S., Baranowski, S., 2006. Magnetic sensor array for investigations of magnetic field distribution, *J. Electrical Engineering*, vol.57, no.8/S, pp.185-188.

Yagitani, S., Okumura, E., Nagano, I., Yoshimura, Y., 2007. Localization of low-frequency source current distributions, *Proc. 2007 Int. Symp. Antennas and Propagation*, pp.89-92.

Yagitani, S., Katsuda, K., Nojima, M., Yoshimura, Y., Sugiura, H., 2011a. Imaging radio-frequency power distributions by an EBG absorber, *IEICE Trans. Commun.*, vol.E94-B, no.8, pp.2306-2315.

Yagitani, S., Katsuda, K., Tanaka, R., Nojima, M., Yoshimura, Y., Sugiura, H., 2011b. A tunable EBG absorber for radio-frequency power imaging, *Proc. 30th URSI GASS*, 4 pages.

Yagitani, S., Sunahara, T., Nakagawa, T., Hiraki, D., Yoshimura, Y., Sugiura, H., 2013. Radio-frequency field measurement using thin artificial magnetic conductor absorber, *Proc. 2013 Int. Symp. Electromagnetic Theory*, 4 pages.

Yamaguchi, M., Yabukami, S., Yurugi, H., Nakada, K., Arai, K. I., Itagaki, A., Itagaki, K., Saito, N., Fuda, K., Watanabe, M., Takahashi, H., Tamogami, T., Sakurada, Y., 1999. Two dimensional electromagnetic noise imaging system using planar shielded-loop coil array, *Proc. 1999 Int. Symp. EMC*, pp.51-54.

Yoshimoto, Y., Taira, K., Sawaya, K., Sato, R., 2005. Estimation of multiple coherent source locations by using SPM method combined with signal subspace fitting technique, *IEICE Trans. Commun.*, vol.E88-B, no.8, pp.3164-3169.